Journal of Clinical Laboratory Analysis 28: 341–348 (2014)

Performance Evaluation of Platelet Counting by Novel Fluorescent Dye Staining in the XN-Series Automated Hematology Analyzers

Yuzo Tanaka,[1] Yumiko Tanaka,[1] Kazumi Gondo,[1] Yoshiko Maruki,[2] Tamiaki Kondo,[2] Satomi Asai,[3] Hiromichi Matsushita,[3] and Hayato Miyachi[3]*

[1]*Clinical Laboratory, Tokai University Hospital, Isehara, Japan*

[2]*Scientific Affairs, Sysmex Corporation, Kobe, Japan*

[3]*Department of Laboratory Medicine, Tokai University School of Medicine, Isehara, Japan*

Background: Conventional automated hematology analyzers have limitations in platelet measurements such as poor accuracy and precision in the low count range and interference by nonplatelet particles. In order to improve it, the newly developed XN-Series automated hematology analyzers (Sysmex Corporation, Kobe, Japan) have been installed with a new dedicated channel for platelet analysis (PLT-F), which is based on a fluorescence flow cytometry method with uses of a novel fluorescent dye specifically staining platelets. We evaluated the basic performance of this new PLT-F channel. *Methods:* Basic performance of the PLT-F channel in within-run reproducibility and assay linearity was studied using standard methods. Correlation was studied between PLT-F and a conventional automated hematology analyzer (XE-2100) and immunoplatelet analysis using anti-CD61 monoclonal antibody (Cell-Dyn Sapphire; Abbott Laboratories). The assay interference by nonplatelet particles such as fragmented red and white blood cells was evaluated by using clinical samples, respectively, from burn injury and acute leukemia. *Results:* Basic performance of the PLT-F platelet counting was satisfactory in within-run reproducibility, linearity and correlation with the conventional analyzer. The correlation was satisfactory also with the immunoplatelet analysis, even for samples from a patient with burn injury, and those with white blood cell fragments displayed, platelet abnormal flag and low platelet counts ($<50 \times 10^9$/l). *Conclusion:* The platelet counting performance of the PLT-F channel of the XN Series had improved accuracy and precision in the low range and in abnormal samples, avoiding the interference by nonplatelet particles. J. Clin. Lab. Anal. 28:341–348, 2014.

Key words: automated hematology analyzer; PLT-F channel; platelet counting; thrombocytopenia; nonplatelet particle

INTRODUCTION

Accurate platelet counting in the low count range is of prime importance for deciding if a platelet transfusion is needed and for monitoring the course of platelet counts after cancer chemotherapy (1,2). There are a number of factors that influence accuracy in platelet counting in the low range by conventional automated hematology analyzers. Among such factors, nonplatelet particles with platelet-sized fragmented red and white blood cells cause falsely high analysis results. In such a case, the platelet count is verified by the manual method or immunoplatelet analysis using anti-CD61 monoclonal antibody (3,4). However, the manual method has problems in skill requirement, assay variation because of skill difference among personnel and a labor-intensive procedure. The immunoplatelet analysis is difficult to use routinely in many medical facilities because of practical reasons such as the requirement of

*Correspondence to: Hayato Miyachi, Department of Laboratory Medicine, Tokai University School of Medicine, 143 Shimokasuya, Isehara, Kanagawa 259–1193, Japan. E-mail: miyachi@is.icc.u-tokai.ac.jp

Received 21 August 2013; Accepted 12 September 2013
DOI 10.1002/jcla.21691
Published online in Wiley Online Library (wileyonlinelibrary.com).

a dedicated analyzer, expensive reagents, and large sample volume of 1 ml or more. To solve these issues, the newly developed XN-Series automated hematology analyzers are equipped with a PLT-F channel, which uses a flow cytometry-based platelet counting method wherein platelets are specifically stained with a novel fluorescent dye, in addition to the PLT-I channel based on an electrical impedance method and the PLT-O channel based on an optical method, which have been provided in the conventional X-Class (XE and XT-Series) analyzers (Sysmex Corporation, Kobe, Japan; (5)). We evaluated the basic performance of the PLT-F channel in platelet counting and the usefulness of this channel in analysis of samples containing interfering nonplatelet particles.

MATERIALS AND METHODS

Samples

Clinical samples used in the study were submitted to the clinical laboratory of Tokai University Hospital for a complete blood count test and sampled during a 6-month period from September 2010 to March 2011. Peripheral blood was taken with addition of EDTA-2K as an anticoagulant. Samples from a concentrated platelet bag for transfusion were used for the linearity study in a high range of platelet count. The study was approved by Institutional Review Board for clinical research of Tokai University Hospital (12R116).

Instruments

The newly developed automated hematology analyzer XN-2000 (XN) was used as an instrument (5). XN counts and classifies blood cells by the DC (direct current) detection method and flow cytometry using a semiconductor laser. In platelet counting by the PLT-F channel, platelets are stained with a fluorescent oxazine dye that is specifically bound with nucleic acid-rich platelet organelles such as ribosomes and mitochondria. They are irradiated with a semiconductor laser beam, and then the forward scattered light and side fluorescence intensities of each platelet are plotted on a 2D scattergram to differentiate and count the platelets (Fig. 1). This technique enables specific differentiation of platelets from other blood cells and interfering particles such as red blood cell fragments. Moreover, the analyzed sample volume of the PLT-F channel is about five times larger than those of conventional methods, in order to obtain highly precise data even with low platelet count samples. XN also measures PLT-I and PLT-O by the electric impedance and optical methods, respectively. We used an automated hematology analyzer XE-2100 (XN) for comparison with XN. Cell-Dyn Sapphire (CD61 method, Abbott Diagnotics, Lake Forest, IL), an immunological platelet analysis system with use of FITC-labeled mouse monoclonal antibody against the platelet membrane glycoprotein GPIIIa (CD61), a recommended international reference method, was used as the reference (3).

Within-Run Reproducibility

Within-run reproducibility was evaluated using samples with three concentrations (low, normal, and high), and coefficient of variation (CV%) continuously measured ten times was determined. The CV continuously measured five times was calculated using samples with a low platelet count ($\leq 50 \times 10^9$/l) and positive for "PLT abnormal distribution" flag ($n = 3$).

Assay Linearity

Assay linearity of a high range was evaluated, using a nine-point dilution series of a sample made from a concentrated platelet bag for transfusion with CELLPACK DCL, the diluent specific for XN. For evaluating linearity in a low range, a healthy patient sample was diluted with CELLPACK DCL to prepare an 11-pont dilution series. Samples of each dilution level were measured three times and the mean value was used for evaluation.

Storage Stability

Samples ($n = 3$) from healthy patients were stored at either 4°C or room temperature, and the storage stability of PLT-F was examined from collection to after 48 h. Samples ($n = 3$) with a low platelet count ($\leq 100 \times 10^9$/l) were stored at room temperature, and their storage stability from collection to after 7 h was studied.

Correlation With XE-2100

The correlation of platelet counts was studied for PLT-I (XE) versus PLT-I (XN), PLT-O (XN), and PLT-F (XN), and also was studied for PLT-O (XE) versus PLT-I (XN), PLT-O (XN), and PLT-F (XN) using samples ($n = 764$ and $n = 35$, respectively) that did not trigger the "PLT abnormal distribution" flag in the XE analysis. To ascertain causes of the discrepancy in platelet counts between different methods, the distribution patterns of XN PLT-F and RET scattergrams, which measured reticulocytes and PLT-O, were examined.

Correlation With Immunoplatelet

Correlation of platelet counts was studied for CD61 versus PLT-I (XE, $n = 21$) and CD61 versus PLT-I (XN), PLT-O (XN), and PLT-F (XN, $n = 21$) using samples of

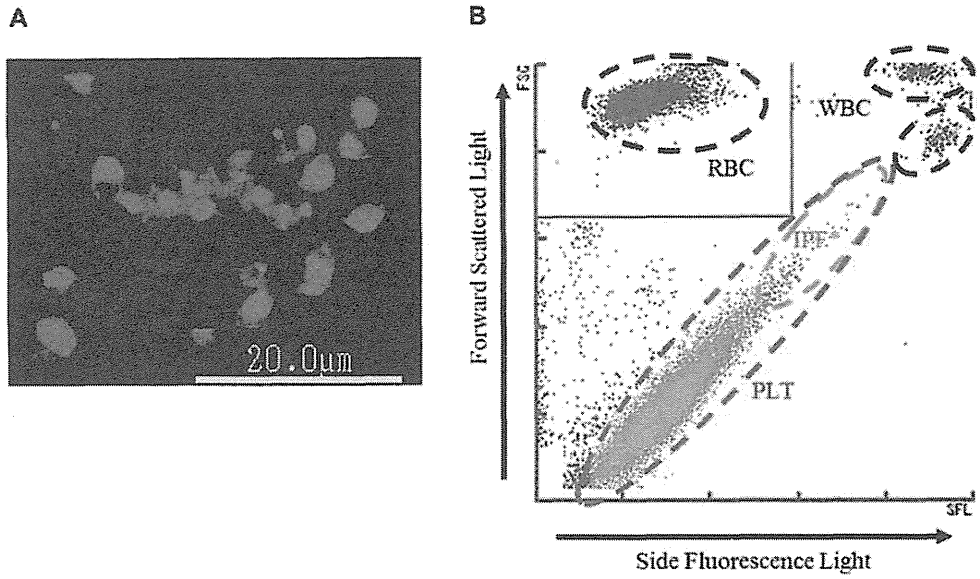

Fig. 1. Principle of PLT-F channel. (A) Platelets stained with the dedicated reagent of PLT-F (fluorescent microscopy image). The staining pattern of platelets by the fluorescent dye is localized, reflecting its specific binding to nucleic acid-rich organelles. (B) PLT-F scattergram. After platelets are stained with fluorescence dye (A), they are differentiated using information from the forward scattered light and side fluorescence intensity (B).
* IPF, immature platelet fraction.

a platelet count $\leq 50 \times 10^9$/l (XE) that did not trigger the "PLT abnormal distribution" flag in XE. Correlation of platelet counts was also studied for CD61 versus PLT-I (XE, $n = 42$) and CD61 versus PLT-I (XN), PLT-O (XN), and PLT-F (XN, $n = 45$) using samples that triggered the "PLT abnormal distribution" flag in XE. The correlation was also studied using selected samples of a platelet count $\leq 50 \times 10^9$/l among the above (XN, $n = 13$; XE, $n = 12$).

Performance Evaluation of PLT-F Channel in the Analysis of Abnormal Samples

The assay performance of PLT-F channel in the analysis of abnormal samples containing white and red cell fragments was evaluated. Platelet counts measured by CD61 of samples from two patients with acute leukemia at initial diagnosis, which had a large number of small (platelet-sized) to large white blood cell fragments, were compared with PLT-I (XN), PLT-O (XN), and PLT-F (XN) counts. The within-run reproducibility of samples ($n = 8$) collected from a patient with burn injury, which had small red blood cell fragments, was examined by PLT-F and the measurement was continuously repeated five times in each sample. The correlation of platelet counts was studied for CD61 versus PLT-I (XE) and CD61 versus PLT-I (XN), PLT-O (XN), and PLT-F (XN) using samples ($n = 32$) from a patient with burn injury. Samples from a burn injury patient were analyzed for the platelet count at different time points during the clinical course by CD61 versus PLT-I (XE), PLT-I (XN), PLT-O (XN), and PLT-F (XN) to examine the influence of fragmented red blood cell on the platelet count by each method.

RESULTS

Within-Run Reproducibility

The CV of samples of the three different concentrations studied (41.3, 245.0, and 886.3 $\times 10^9$/l by PLT-F) was in the range 1.0–4.6% for PLT-I, 1.6–6.3% for PLT-O, and 0.7–1.6% for PLT-F, the CVs remaining small throughout the low to high ranges of concentration. The comparison of the three methods showed that the within-run reproducibility was best (the CV was smallest) with PLT-F. The CV of the three samples with low platelet counts that had triggered the "PLT abnormal distribution" flag in the XE was in the range 10.9–27.9% for PLT-I, 3.3–11.4% for PLT-O, and 1.9–8.3% for PLT-F. Thus, the PLT-F had the best within-run reproducibility.

Assay Linearity

The dilution linearity was shown in high platelet concentrations ranged up to 3,800 $\times 10^9$/l for PLT-I ($y = 0.9888x + 19.946$), 3,510 $\times 10^9$/l for PLT-O ($y = 0.993x + 28.725$), and 4,132 $\times 10^9$/l for PLT-F ($y = 0.9882x + 2.2539$). The dilution linearity was also shown in the low platelet concentration range of 4–45 $\times 10^9$/l for PLT-I ($y = 0.9882x + 0.849$), 4–46 $\times 10^9$/l for PLT-O ($y = 1.0118x$

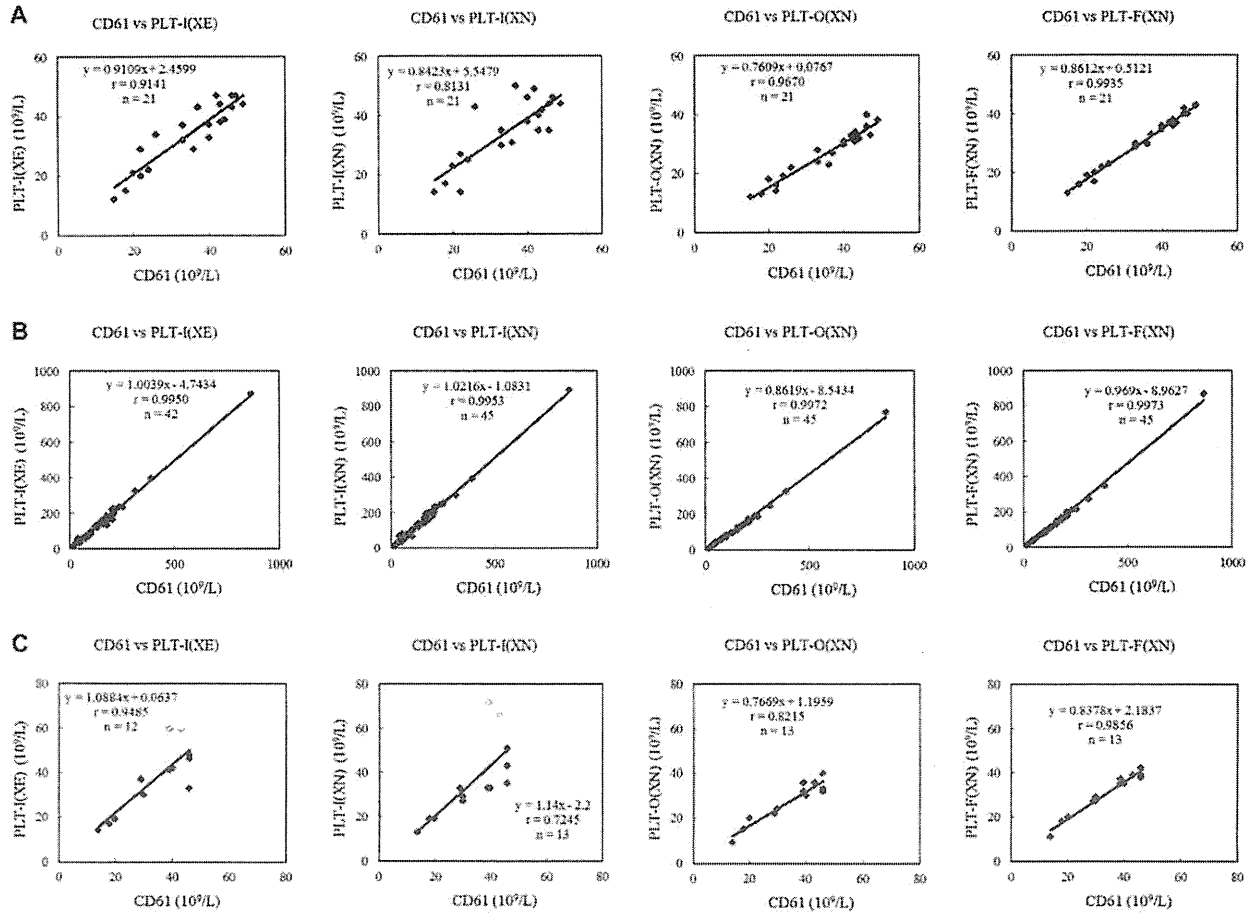

Fig. 2. Correlation of platelet counts between CD61 and XN. (A) Samples that did not display the "PLT abnormal distribution" flag and had a platelet count below 50 × 10^9/l. (B) Samples that displayed the "PLT abnormal distribution" flag. (C) Samples with a platelet count below 50 × 10^9/l among samples that displayed the "PLT abnormal distribution" flag. White dots show results with PLT-I that differed from the CD61 counts by more than 20 × 10^9/l.

+ 0.7396), and 5–46 × 10^9/l for PLT-F ($y = 0.9812x - 0.3103$). Thus, the PLT-F method showed good linearity, the line passing closer to the origin, as compared to PLT-I and PLT-O in the low and high count ranges.

Storage Stability

Platelet counting of the three samples taken from healthy patients remained stable up to 48 h at both 4°C and at room temperature. Even samples with low platelet counts were stable for 7 h after collection (data not shown).

Correlation With XE-2100

The correlation of the platelet counts of samples that did not trigger the "PLT abnormal distribution" flag was good, the correlation coefficients (*rs*) being respectively 0.979, 0.966, and 0.968 for PLT-I (XE) versus PLT-I (XN), PLT-O (XN), and PLT-F (XN), and 0.991, 0.988, and 0.989 for PLT-O (XE) versus PLT-I (XN), PLT-O (XN), and PLT-F (XN).

Correlation With Immunoplatelet

The correlation coefficients (*rs*) of platelet counts measured by CD61 versus the three methods in XN using samples ($n = 21$) that had a platelet count below 50 × 10^9/l and did not show "PLT abnormal distribution" flag in XE were, respectively, 0.813, 0.967, and 0.994 for PLT-I (XN), PLT-O (XN), and PLT-F (XN). Thus, the correlation was highest with PLT-F (Fig. 2A). Correlation with CD61 revealed *r* values of 0.995, 0.997, and 0.997 for PLT-I (XN), PLT-O (XN), and PLT-F (XN), respectively, with samples that triggered the "PLT abnormal distribution" flag in XE (Fig. 2B). There was not much difference among

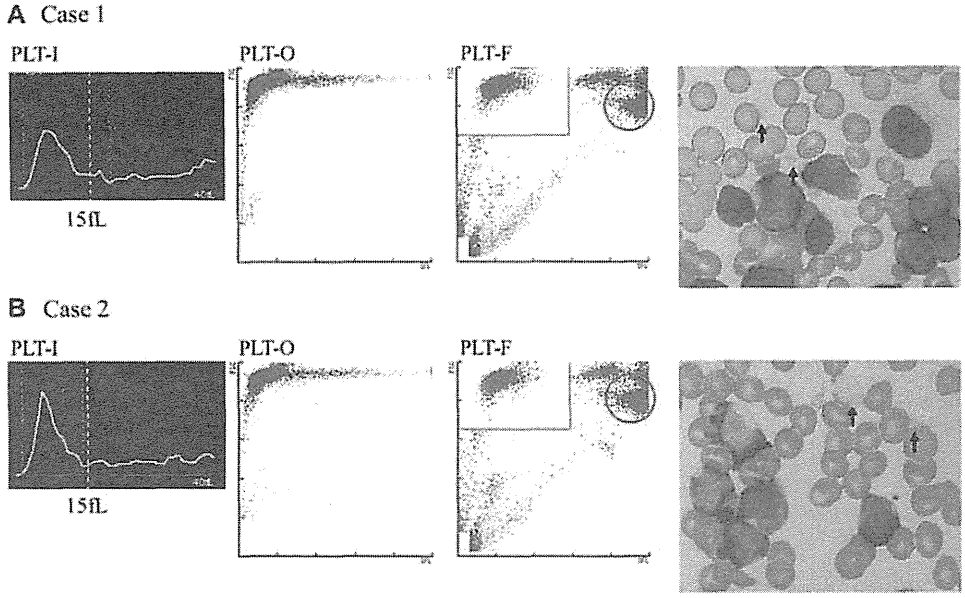

Fig. 3. Histograms (PLT-I) and scattergrams (PLT-O and PLT-F) of samples appeared white blood cell fragments. Dashed line in the PLT-I histogram shows platelet volume 15 fL. In PLT-F scattergram, the boundary line between the PLT and WBC areas is in the zone between them with few dots of particles. The part circled with the red line is believed to be where white blood cell fragments are plotted.

the correlation coefficients for platelet counts by CD61 versus the three methods in XN. However, for samples with a platelet count below 50×10^9/l, the corresponding r values were 0.725, 0.822, and 0.986, respectively, for PLT-I (XN), PLT-O (XN), and PLT-F (XN, Fig. 2C). With PLT-I, two samples gave results that differed from the CD61 counts by more than 20×10^9/l (Fig. 2C, white dots). The XN RET scattergram, which counted the reticulocyte, showed dots in the fragmented red blood cell and microcytic red blood cell areas, and the "fragments" flag was displayed. The PLT-F scattergram did not show any interfering particles in the platelet area.

Performance Evaluation of PLT-F Channel in the Analysis of Abnormal Samples

The platelet count of a sample from a patient with acute leukemia (Case 1) was 11×10^9, 26×10^9, 20×10^9, and 15×10^9/l by CD61, PLT-I, PLT-O, and PLT-F, respectively. The peripheral blood had small fragments of the white blood cell but only a flag warning of low platelet count was displayed in XN analysis. The platelet dots were dispersed in the RET scattergram of XN, and contamination of white blood cell fragments could not be ruled out. The fragments of white blood cell were plotted in the WBC area of the PLT-F scattergram, with no intrusion into the immature platelet fraction (IPF) area. The platelet count by PLT-F matched with that by CD61 (Fig. 3). The platelet count of a sample from another patient with acute leukemia (Case 2) was 15×10^9, 25×10^9, 19×10^9, and 7×10^9/l, by CD61, PLT-I, PLT-O, and PLT-F, respectively. The peripheral blood showed white blood cell fragments that were larger or smaller than red blood cells. Flags warning of low platelet counts, platelet aggregation, and abnormal RET scattergram were displayed in XN. The white blood cell fragments were seen as an abnormal cluster above the IPF area of high fluorescence intensity in the PLT-F scattergram, and this cluster was recognized as white blood cells. The platelet count by PLT-F was slightly lower than the CD61 count, and influence of white blood cell fragments could not be found (Fig. 3). On the other hand, in the PLT histogram curve showed some fluctuations in the region representing cells with volume larger than 15 fL (Fig. 3, dashed line in the PLT-I histogram).

In the performance evaluation of the PLT-F method, using samples from a burn injury patient, the within-run reproducibility of the PLT-F counts was good (CV 1.2–4.4%), the CV being small even in samples with a low platelet count (Table 1). The correlation of the PLT counts measured by CD61 and other methods was the highest with PLT-F (XN, $r = 0.979$), and the slope of the regression equation was also close to 1 (Fig. 4A). As for the monitoring of changes in the platelet count with samples from the burn injury patient, both the PLT-I and PLT-O methods gave results considerably different from those of CD61 soon after the injury because of the influence of fragmented red blood cells and microcytes. However, these differences decreased gradually with time and no influence of the contamination of red blood cell

TABLE 1. Within-Run Reproducibility of Platelet Counts by PLT-F Method in Analysis of Samples From a Burn Injury Patient

	Platelet counts by PLT-F method ($\times 10^9$/l)					
Sample no.	Max	Min	Range	Mean	SD	CV%
1	21	20	1	20.2	0.4	2.0
2	33	30	3	32.0	1.4	4.4
3	43	42	1	42.4	0.5	1.2
4	75	72	3	73.2	1.3	1.8
5	83	80	3	81.4	1.1	1.4
6	156	151	5	153.2	1.9	1.2
7	167	162	5	164.2	1.9	1.2
8	173	168	5	171.2	2.2	1.3

$n = 5$.

fragments was seen after day 4. On the other hand, the platelet counts by PLT-F corresponded with those by CD61 throughout the study period (Fig. 4B).

DISCUSSION

We evaluated the basic analytical performance of the newly dedicated platelet counting channel, the PLT-F, of the automated hematology analyzer XN-2000. As for the within-run reproducibility, the CV of PLT-F counts was small compared to PLT-I and PLT-O and the difference was more clear in the low platelet count samples. Dilution linearity was confirmed over a wide range, from low to high platelet counts, in PLT-F as in other analysis methods.

CD61 immunological platelet analysis method is a highly platelet specific method that uses a monoclonal antibody against the platelet membrane protein GPIIIa (CD61), and is a recommended international standard method (6,7). CD61 has been reported to give results that are highly correlated with those of the manual method (Brecher–Cronkite method) even in samples with a low platelet count ($\leq 50 \times 10^9$/l). Among the various methods tested here, PLT-F gave higher correlation with CD61 compared to PLT-I and PLT-O for samples with a platelet count $\leq 50 \times 10^9$/l. Moreover, the PLT-F method showed good linearity, the line passing close to the origin. This seems to be because of better accuracy of the PLT-F method compared to PLT-I and PLT-O in the low count range. Samples that showed a discrepancy $\geq 20 \times 10^9$/l between CD61 and PLT-I counts with XN analyzers displayed the "fragments" flag, which indicated the presence of fragmented red blood cells or microcytes, and these appear to have interfered with the platelet counting in the PLT-I channel.

Nonplatelet particles that can cause falsely high platelet counts include white and red cell fragments. White blood cell fragments are often seen in cases where there is an extreme increase in white blood cells, such as in leukemia. Quite often these fragments are of about the same size as platelets, resulting in falsely high platelet counts by PLT-I and PLT-O (4, 8). Among the PLT-I, PLT-O, and PLT-F platelet counting of samples with white blood cell fragments studied here, the counts by PLT-I were the highest in comparison to CD61. In the platelet histogram, the curve formed a shoulder followed by an irregularly wavy pattern in the region of cells larger than 15 fL. This suggested the possibility of white blood cell fragments being counted as platelets. The PLT-O method gave slightly higher platelet counts than CD61. The platelet count of Case 1 determined by PLT-F matched with that by CD61. The PLT-F platelet count of Case 2 was slightly lower than by CD61. In the scattergram, the boundary between the platelets and white blood cell fragments passed through an area where only a few dots were plotted. Thus, there was no abnormality in the manner of defining the borderline, and the cause of the low platelet count of Case 2 could not be identified. Nevertheless, the two cases studied here did not give falsely high counts in the PLT-F analysis. This result suggested that platelet analysis by PLT-F could possibly avoid the influence of white blood cell fragments. These results point to the need for further investigations with a larger number of cases to determine "optimal algorithms and differentiation criteria" for discriminating white blood cell fragments from platelets.

The PLT-I and PLT-O counts of samples from patients with burn injury are often falsely high because of the small fragmented red blood cells are inadvertently registered as platelets. In contrast, the immunological method of platelet counting is useful for samples of burn injury cases as it is not affected by nonplatelet particles like small fragmented red blood cells, and gives accurate platelet counts. In the present study, the counts by PLT-I and PLT-O appeared to be falsely high, as they were much higher than those of CD61. In monitoring of the burn injury case, the platelet counts of the CD61 and PLT-F methods were quite similar whereas the PLT-I and PLT-O counts remained higher than them up to day 4. These results confirmed that in the analysis of burn injury samples, the PLT-F method was not influenced by small fragmented red blood cells, a cause of falsely high values, and gave results similar to those of CD61. Furthermore, PLT-F counting of samples from burn injury patients had good within-run reproducibility, the CV being small.

We believe the improved accuracy and precision of platelet counting with the PLT-F over the PLT-O analysis of samples containing interfering nonplatelet particles is due to the difference of specificity to platelets between fluorescent dyes, oxazine, and polymethine, respectively. The nonspecific binding of the latter to the cellular membrane has been a cause of falsely counting of the

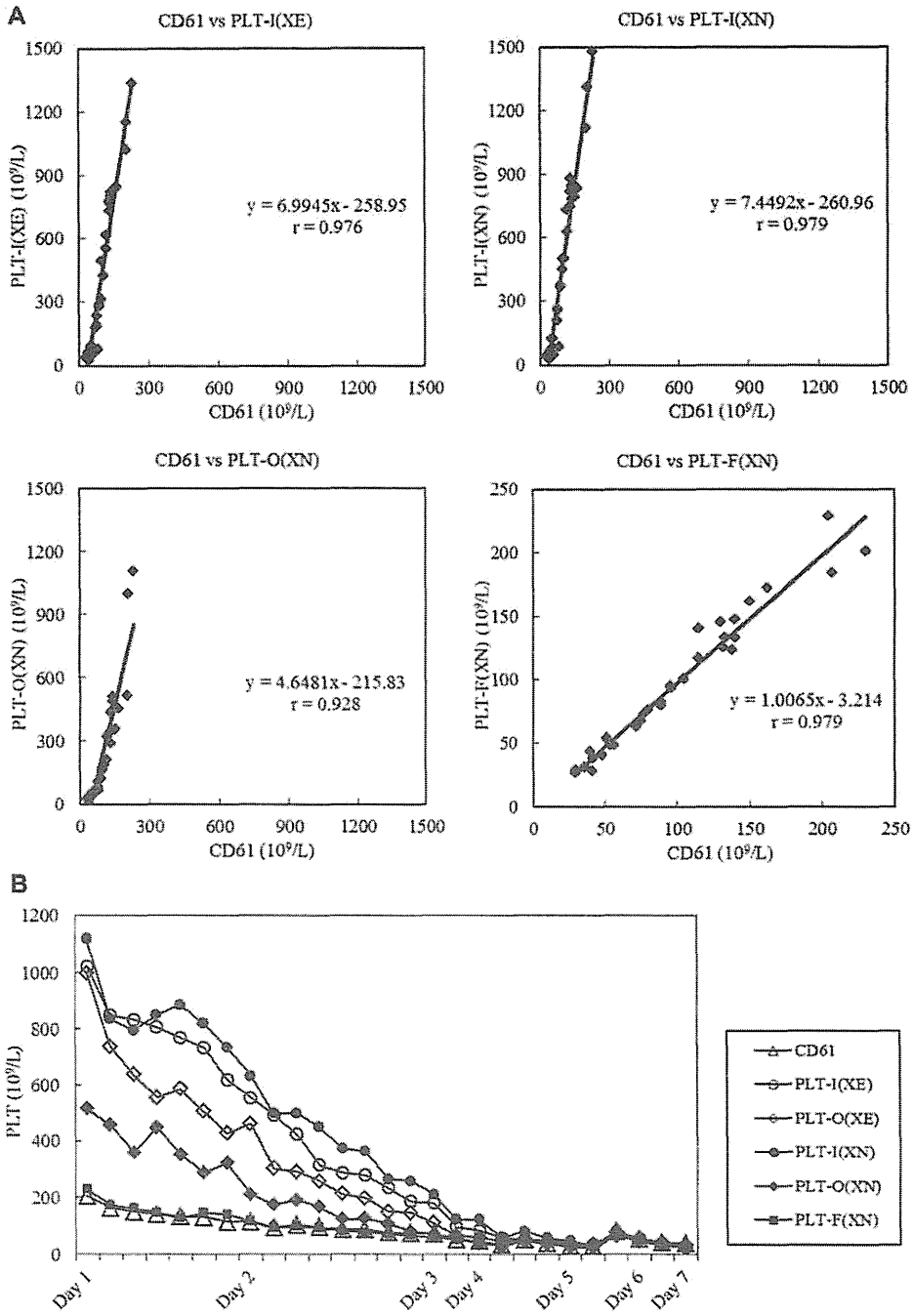

Fig. 4. Correlation with CD61 platelet counts and monitoring of platelet counts in samples from burn injury patients. (A) Correlation of platelet counts between CD61 and XN using samples from burn injury patients. (B) Monitoring of platelet counts in burn injury samples.

small fragmented red blood cells as the platelets, which has been minimized in the former.

With the XE analyzer, when "PLT abnormal distribution" flag appears in the PLT-I analysis, a message prompting analysis by PLT-O is displayed. With such samples, the PLT-O analysis is additionally carried out through the RET channel. However, there is often considerable discrepancy between the PLT-I and PLT-O counts. The reporting of platelet counts relies on automatic assessment by the analyzer's switching function, which selects one of the two methods (9, 10). In our laboratory, when the cause of such a difference cannot be ascertained

by observation of the blood smears, the platelet counting is performed by a manual method (indirect method) for confirmation. When the difference is considerably large, the CD61 immunological analysis is also carried out and the results are reported. In such types of samples, the additional handy procedure of PLT-F analysis would allow us to report accurate platelet counts.

The operation of the analyzer for PLT-F analysis is simple, rapid, and inexpensive, and the required sample volume is small (88 μl). PLT-F analysis obviates a need for the dedicated equipment and expensive reagents required for an immunological method. It can be employed for routine testing to provide rapid analysis and reporting on a 24-h basis. Therefore, the analyzer would contribute to more appropriate clinical decision making such as in blood transfusion, as it provides highly accurate and rapid platelet counting, and would be useful for efficient operation of hematological or clinical laboratories. This is supportive of a previous report on the performance evaluation of the XN series, which has suggested that the analyzer improves confidence of results and workflow efficiency in a routine hematology laboratory (5).

In conclusion, the performance evaluation of the platelet counting of PLT-F, a new function of the automated hematology analyzers XN-Series, confirmed that it could provide better precision and accuracy of analysis for low platelet counts and even with abnormal samples, avoiding the interference by nonplatelet particles such as that in burn injury and leukemia.

ACKNOWLEDGMENTS

We thank Kazutoyo Sakairi, Mitsuko Ota, Nagisa Nakazawa, and Takayuki Seto working in Clinical Laboratory of Tokai University Hospital, for their contribution in performing the research by technical support in the measurement of clinical samples.

REFERENCES

1. Segal HC, Briggs C, Kunka S, et al. Accuracy of platelet counting haematology analysers in severe thrombocytopenia and potential impact on platelet transfusion. Br J Haematol 2005;128: 520–525.
2. Saliba RM, Komanduri KV, Giralt S, et al. Leukemia burden delays lymphocyte and platelet recovery after allo-SCT for AML. Bone Marrow Transplant 2009;43:685–692.
3. Trabuio E, Valverde S, Antico F, Manoni F, Gessoni G. Performance of automated platelet quantification using different analysers in comparison with an immunological reference method in thrombocytopenic patients. Blood Transfus 2009;7:43–48.
4. Gill JE, Davis KA, Cowart WJ, Nepacena FU, Kim YR. A rapid and accurate closed-tube immunoassay for platelets on an automated hematology analyzer. Am J Clin Pathol 2000;114: 47–56.
5. Briggs C, Longair I, Kumar P, Singh D, Machin SJ. Performance evaluation of the Sysmex haematology XN modular system. J Clin Pathol 2012;65:1024–1030.
6. Harrison P, Ault KA, Chapman S, et al. An interlaboratory study of a candidate reference method for platelet counting. Am J Clin Pathol 2001;115:448–459.
7. Grimaldi E, del Vecchio L, Scopacasa F, et al. Evaluation of the platelet counting by Abbott CELL-DYN SAPPHIRE haematology analyser compared with flow cytometry. Int J Lab Hematol 2009;31:151–160.
8. Li S, Salhany KE. Spurious elevation of automated platelet counts in secondary acute monocytic leukemia associated with tumor lysis syndrome. Arch Pathol Lab Med 1999;123:1111–1114.
9. Briggs C, Kunka S, Machin SJ. The most accurate platelet count on the Sysmex XE-2100. Optical or impedance? Clin Lab Haematol 2004;26:157–158.
10. Briggs C, Harrison P, Grant D, Staves J, MacHin SJ. New quantitative parameters on a recently introduced automated blood cell counter—The XE 2100. Clin Lab Haematol 2000;22:345–350.

International Journal of Laboratory Hematology
The Official journal of the International Society for Laboratory Hematology

Letter to the Editor

Elimination of interference by lipids in the low WBC mode in the automated hematology analyzer XN-2000

Sir, The dissemination of chemotherapy in various malignancies and expanded application of stem cell transplantation have currently made more chances for the physicians to take care of the patients with leukopenia [1, 2]. There is a demand for immediate and reliable data for the low counts of white blood cells (WBC) in automated hematology analyzers. However, the measurement of WBC counts and differentials has a limitation in the accuracy in leukopenia. Particularly spuriously high counts by the contamination of nucleated erythrocytes (NRBC) and lipids are problematic in the care of the leucopenia patients [3]. Conventional analyzers usually use scattered lights or direct-current electricity to count WBC, and thus, the intensities are subject to interference from such a non-WBC particle.

The newly developed automated hematology analyzers XN-series (Sysmex Corp., Kobe, Japan) have several modifications for the reliability of measurement by optimization of the reagent reactions, the signal processing, and the analysis algorithms: The contamination of NRBC in the measurement of WBC counts is eliminated using WNR channel, and the accurate WBC differentials are provided using WDF channel [4]. Using fluorescence staining for nucleic acid and scattered light, both measurement channels exclude the interference such as lipid, nonlysed RBCs, and so on. Furthermore, using the WDF channel, the XN-series are also equipped with the low WBC (LW) mode, which is intended for measurement of a low range of WBC count and differentiation by counting threefold sample volume [4].

We have evaluated the assay performance of WBC counting of XN-2000 in a low range by comparing the LW and the normal measurement mode (Whole blood mode: WB mode), the conventional analyzer XE-2100 (Sysmex Corp.), and the manual method.

Clinical samples used in the study were submitted to the clinical laboratory of Tokai University Hospital for a complete blood count test and sampled during a 6-month period from September 2010 to March 2011. Peripheral blood was taken with addition of EDTA-2K as an anticoagulant. The study was approved by Institutional Review Board for Clinical Research of Tokai University Hospital (12R116) and Sysmex Corp.

When the within-run reproducibility in 10 samples with a LW count ($<1.40 \times 10^9$/L, three of them were $<0.13 \times 10^9$/L) was determined in 5 or 10 replicates, the LW mode had better within-run reproducibility of WBC counting than the WB mode, with the coefficients of variation (CV%) being 0.6–7.7% and 1.6–11.2%, respectively. The LW mode also provided better within-run reproducibility than the WB mode in the analysis of the absolute numbers of each cell fraction of WBC in neutrophil and lymphocyte, with the CV being <15% in the LW mode, as long as the absolute count of each differential fraction was more than 0.10×10^9/L (data not shown). This improvement in the measurement reproducibility in LW mode is confirmatory of WBC counting using threefold more cells in the samples in comparison with the WB mode. The LW mode showed the linearity of WBC counting in a range $0.01–1.15 \times 10^9$/L ($y = 0.990x + 0.002$, $r = 0.9997$), when evaluated with an eleven-step dilution series using the diluent CELLPACK (Sysmex Corp.). The linearity was also seen in each WBC differential measured by the LW and WB modes: $0.01–0.33 \times 10^9$ and $0.02–0.33 \times 10^9$/L for neutrophils, $0.01–0.61 \times 10^9$ and $0.05–0.56 \times 10^9$/L for lymphocytes.

Then, we evaluated the interference of lipid particles for WBC counting by the addition of fat emulsion to a sample from a healthy volunteer. XN-2000 WNR and WDF channel for WB and LW mode could accurately count WBC by distinguishing it from the lipids (Figure 1a and b). On the other hand, XE-2100 showed false elevation of WBC counts, with a curved strand of 'Lissajous-like pattern' plots in the scattergram (Figure 1b) [5, 6].

The method comparison for WBC counting between the LW and WB modes in XN-2000 and XE-2100 showed good correlation in the range of $<1.40 \times 10^9$/L (293, 298 and 294 samples, respectively; Figure 2a). However, 8 of the samples showed discrepancy in the

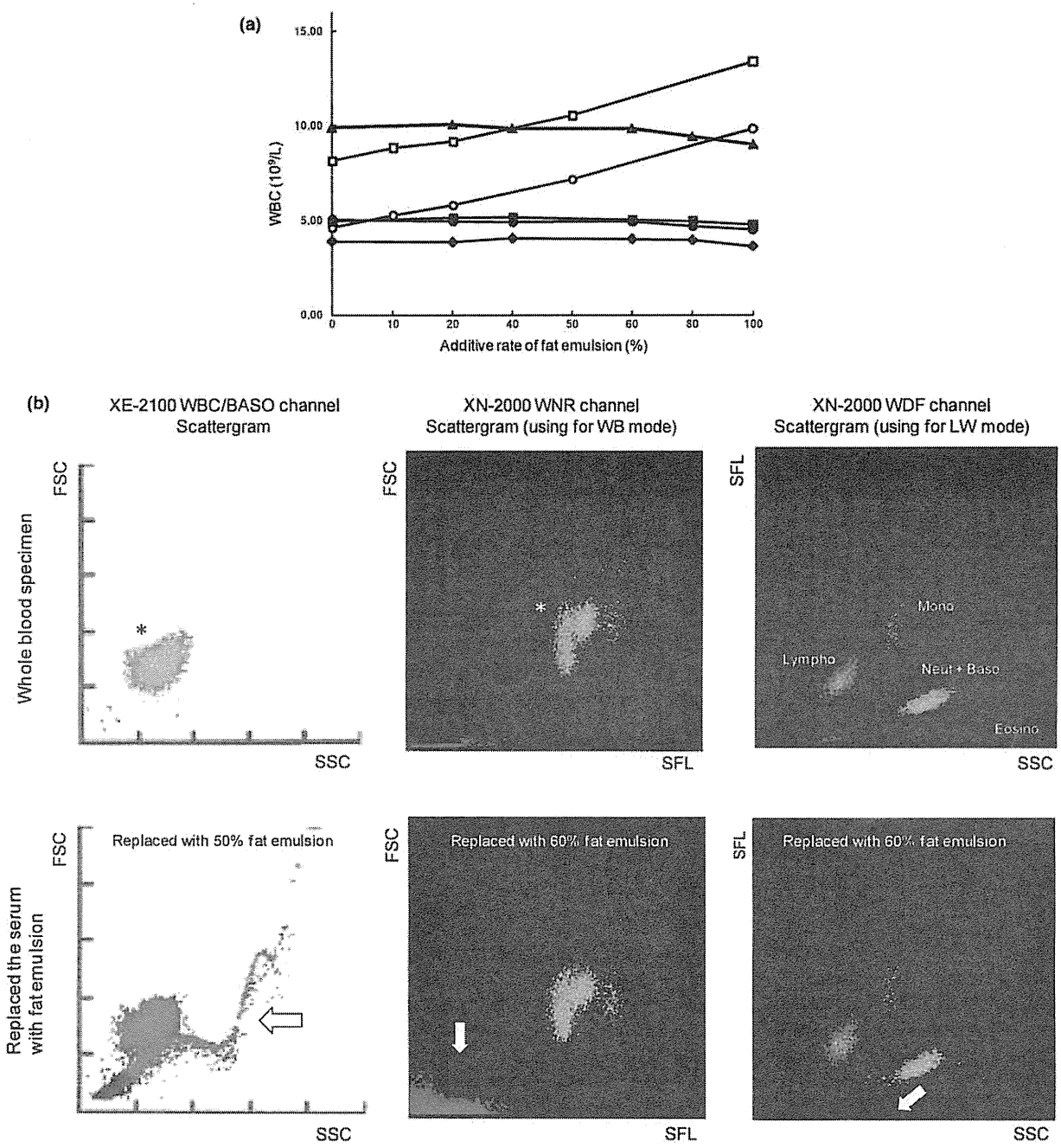

Figure 1. Evaluation of lipid interference for white blood cells (WBC) counting. (a) The six peripheral blood samples of which plasma were partially replaced (0%, 10%, 20%, 40%, 50%, 60%, 80%, or 100%) by intravenous fat emulsion (Intralipid® 20%, Fresenius Kabi Japan K.K.) were measured by WNR channel [for whole blood (WB) mode] (■, ●), WDF channel [for low WBC (LW) mode] (▲, ♦) of XN-2000 or XE-2100 (□, ○). (b) The pattern of scattergrams with or without addition of the fat emulsion. (*) and white arrow shows the WBC cluster and characteristic plots in an each specimen containing lipid particles.

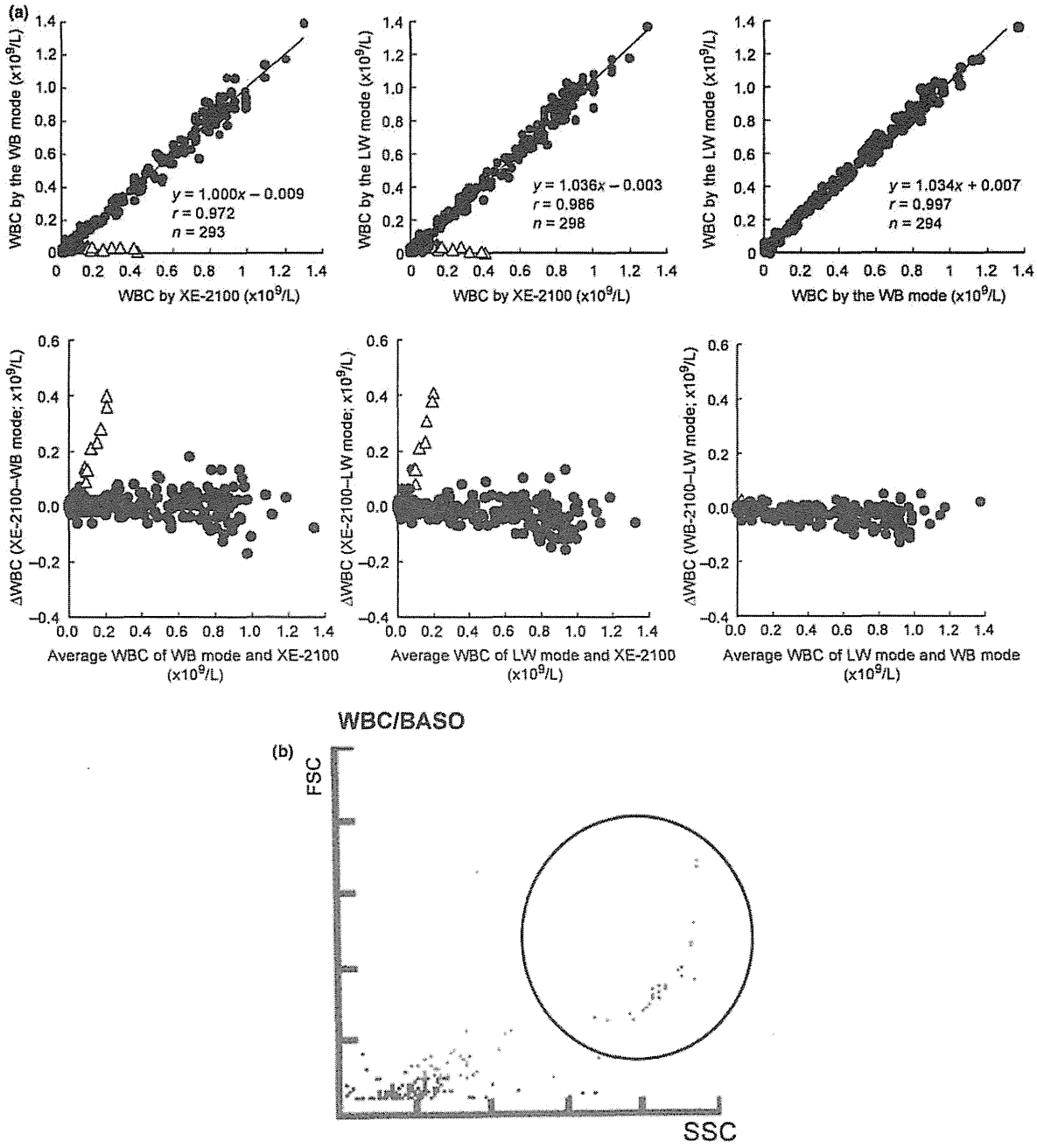

Figure 2. (a) The relationship between white blood cells (WBC) counts measured by XN-2000 and XE-2100. The relationships between WBC counts between the whole blood (WB) mode and XE-2100, the low WBC (LW) mode and XE-2100, and the LW and WB modes in XN-2000 are shown (upper graphs). The white triangles (△) represent a sample that has a discrepant WBC count between XN-2000 and XE-2100. And each Bland–Altman plots is shown in lower. (b) An example of a WBC/BASO scattergram evaluated by XE-2100. The abnormal distribution of a strand of dots appeared as 'Lissajous-like pattern' (○), generating a falsely high count, was recognized only in the XE-2100 analysis.

measured WBC counts by XN-2000 (the LW or WB modes) and XE-2100. All the 8 discrepant cases showed higher values of WBC counts up to 0.41×10^9/L in XE-2100 than those measured by XN-2000, which were all below 0.06×10^9/L actually. The WBC counts by XN-2000 agreed with those determined with the standard manual method by one person using Turk's solution and the Fuchs-Rosenthal chamber, which were from 0.003 to 0.069×10^9/L (0.003×10^9/L in 5 samples, 0.009, 0.031, and 0.069×10^9/L in each), suggesting spuriously high WBC counts in XE-2100. The WBC/BASO scattergram of XE-2100 generated abnormal distribution in all the discrepant samples, with the 'Lissajous-like pattern' (Figure 2b) [5–7]. The WBC/BASO channel of XE-2100 differentiates various cells according to size and morphological information obtained from the forward and side scatter light signals. The lipids generate particles large enough that are not correctly differentiated from blood cells because of their similarity in optical information. XE-2100 performs WBC classification using nucleic acid staining, so it could provide accurate WBC count from the differential channel. However, the result from that channel is for only service data in XE-2100.

The spuriously high WBC counts by automated hematology analyzers are caused by the contamination of cellular and noncellular particles originating from the specimen [3]. In the current study, it was found that the abnormal clusters due to noncellular particles such as lipids have been cleared from both their WNR and WDF channels for WBC analysis. This improvement is confirmatory of the principle for fractionating WBC in XN-Series, where a fluorescent dye with a high affinity to nucleic acids has been introduced, theoretically enabling the discrimination of WBC from non-WBC particles such as lipids [4]. Therefore, we considered lipemia specimens no longer interfere with WBC counting using XN analyzer.

The method comparison study using 25 samples with an extremely LW range $<0.10 \times 10^9$/L revealed that WBC counts by the LW and the WB modes had moderate correlation with the manual method, with a regression line being $y = 0.5828x + 0.015$ ($r = 0.7829$) and $y = 0.6424x + 0.0156$ ($r = 0.7358$), respectively. A combination of the low slope and the positive interception suggests more influences of falsely high values on the lower range of WBC. In all the samples, the WNR scattergram of XN-2000 displayed no apparent abnormal clusters. In such a case, influences by the carryovers from the previous analysis might be also considered.

In contrast to the WB mode, the LW mode dose not discard the differential data even in the extremely LW range ($0.01–0.1 \times 10^9$/L), and the absolute numbers as well as the proportion of each cell fraction are displayed. As the reference method for comparison, differential WBC counts were determined with the manual method by one person, where 10–100 cells were counted in May-Grunwald-Giemsa-stained smears of samples having 0.003×10^9/L or more WBC counts. The method comparison study using 29 samples with WBC $<0.10 \times 10^9$/L revealed that data for differentials displayed only by the LW mode had moderate correlation with the manual method for neutrophil and lymphocyte counting with a regression line being $y = 1.1039x + 0.0123$ ($r = 0.8730$) and $y = 0.668x + 0.0037$ ($r = 0.7903$), respectively. These suggest that the absolute numbers of neutrophil or lymphocyte counts generated by the LW mode could be used as immediate and reliable data, as supported by improvement in precision and accuracy in terms of elimination of the interference by noncellular particles.

In conclusion, evaluation of the analytical performance of the newly developed automated hematology analyzer XN-2000 for the WBC counting in a low range revealed that a spuriously high count due to the interference by the contamination of lipids had been eliminated. Furthermore, the LW mode, which was newly equipped in the analyzer, had better performance than the WB mode in precision as evaluated by within-run reproducibility for a low range of WBC counts down to 0.10×10^9/L, and the WBC differentials for neutrophil and lymphocyte were reportable with moderate correlation with the manual method for an extremely low range of WBC counts $<0.10 \times 10^9$/L. The LW mode of XN-2000 can be used as reference for the manual method or in place of it, in a selective manner, depending on the range of WBC counts in leucopenia.

Acknowledgements

We thank Kazutoyo Sakairi, Nagisa Nakazawa, Noriko Wada, Kazumi Gondo, and Takayuki Seto in Clinical Laboratory of Tokai University Hospital for their contributing to performing the research by technical support in the measurement of clinical samples.

Y. Tanaka*, H. Matsushita†, Y. Tanaka*, Y. Maruki‡, F. Hayashi‡, T. Kondo‡, S. Asai†, H. Miyachi†

Clinical Laboratory, Tokai University Hospital, Isehara, Japan
†*Department of Laboratory Medicine, Tokai University School of Medicine, Isehara, Japan*
‡*Scientific Affairs, Sysmex Corporation, Kobe, Japan*
E-mail: miyachi@is.icc.u-tokai.ac.jp

doi: 10.1111/ijlh.12163

References

1. Passweg J, Halter J, Bucher C, Gerull S, Heim D, Rovó A, Buser A, Stern M, Tichelli A. Hematopoietic stem cell transplantation: a review and recommendations for follow-up care for the general practitioner. Swiss Med Wkly 2012;142:w13696.
2. Schmidt M, Koelbl H. Adjuvant chemotherapy in early breast cancer. Minerva Ginecol 2012;64:53–65.
3. Zandecki M, Genevieve F, Gerard J, Godon A. Spurious counts and spurious results on haematology analysers: a review. Part II: white blood cells, red blood cells, hemoglobin, red cell indices and reticulocytes. Int J Lab Hematol 2007;29:21–41.
4. Briggs C, Longair I, Kumar P, Singh D, Machin SJ. Performance evaluation of the Sysmex haematology XN modular system. J Clin Pathol 2012;65:1024–30.
5. Doornbos RM, Hoekstra AG, Deurloo KE, De Grooth BG, Sloot PM, Greve J. Lissajous-like patterns in scatter plots of calibration beads. Cytometry 1994;16:236–42.
6. Hoekstra AG, Doornbos RM, Deurloo KE, Noordmans HJ, Grooth BG, Sloot PM. Another face of Lorenz-Mie scattering: monodisperse distributions of spheres produce Lissajous-like patterns. Appl Opt 1994;33:494–500.
7. Mori Y, Mizukami T, Hamaguchi Y, Tsuruda K, Yamada Y, Kamihira S. Automation of bone marrow aspirate examination using the XE-2100 automated hematology analyzer. Cytometry B Clin Cytom 2004;58:25–31.

GENES, CHROMOSOMES & CANCER 53:299–308 (2014)

The Leucine Twenty Homeobox (*LEUTX*) Gene, Which Lacks a Histone Acetyltransferase Domain, is Fused to *KAT6A* in Therapy-Related Acute Myeloid Leukemia with t(8;19)(p11;q13)

Yoshiaki Chinen,[1] Tomohiko Taki,[2] Yasuhiko Tsutsumi,[1] Satoru Kobayashi,[1] Yosuke Matsumoto,[1] Natsumi Sakamoto,[1] Junya Kuroda,[1] Shigeo Horiike,[1] Kazuhiro Nishida,[1] Hirofumi Ohno,[3] Naokuni Uike,[3] and Masafumi Taniwaki[1]*

[1]Department of Molecular Hematology and Oncology, Kyoto Prefectural University of Medicine Graduate School of Medical Science, Kyoto, Japan
[2]Department of Molecular Diagnostics and Therapeutics, Kyoto Prefectural University of Medicine Graduate School of Medical Science, Kyoto, Japan
[3]Department of Hematology, National Kyushu Cancer Center, Fukuoka, Japan

The monocytic leukemia zinc finger protein *KAT6A* (formerly *MOZ*) gene is recurrently rearranged by chromosomal translocations in acute myeloid leukemia (AML). *KAT6A* is known to be fused to several genes, all of which have histone acetyltransferase (HAT) activity and interact with a number of transcription factors as a transcriptional coactivator. The present study shows that the leucine twenty homeobox (*LEUTX*) gene on 19q13 is fused to the *KAT6A* gene on 8p11 in a therapy-related AML with t(8;19)(p11;q13) using the cDNA bubble PCR method. The fusion transcripts contained 83 nucleotides upstream of the first ATG of *LEUTX* and are presumed to create in-frame fusion proteins. *LEUTX* is known to have a homeobox domain. Expression of the *LEUTX* gene was only detected in placenta RNA by RT-PCR, but not in any tissues by Northern blot analysis. The putative LEUTX protein does not contain any HAT domain, and this is the first study to report that *KAT6A* can fuse to the homeobox gene. The current study, with identification of a new partner gene to *KAT6A* in a therapy-related AML, does not elucidate the mechanisms of leukemogenesis in *KAT6A*-related AML but describes a new gene with a different putative function.

INTRODUCTION

Several leukemias are genetically characterized by the presence of acquired translocations and inversions that result in fusion genes of pathogenetic, diagnostic, and prognostic importance. The 8p11 translocations result in diverse oncogenic fusion genes involving fibroblast growth factor receptor 1 (*FGFR1*) or monocytic leukemia zinc finger protein (*KAT6A*, previously *MOZ* or *MYST3*). *FGFR1* encodes a receptor tyrosine kinase, rearrangements of which have been associated with stem cell leukemia/lymphoma or myeloproliferative neoplasm, whereas *KAT6A* is a member of a histone acetyltransferase family associated with monoblastic and monocytic leukemia (Patnaik et al., 2010). *KAT6A*-related translocations are associated with the same type of acute myeloid leukemia (AML), with blast cells of a monocytoid phenotype having pronounced erythrophagocytic activity. This subtype is found in ~2% of cases of AML with the French-American-British classification M4 or M5 phenotype (Aguiar et al., 1997). The most frequent translocation partner gene for *KAT6A* is *CREBBP* in t(8;16)(p11.2;p13.3) (Borrow et al., 1996), other 8p11 translocations involving *KAT6A* give rise to fusion oncogenes such as *KAT6A-NCOA2* (nuclear receptor coactivator 2, also known as *TIF2* or *GRIP1*) in inv(8)(p11q13) (Liang et al., 1998),

Supported by: a research program of the Project for Development of Innovative Research on Cancer Therapeutics (P-Direct) and a Grant-in-Aid for Scientific Research (C) from the Ministry of Education, Culture, Sports, Science and Technology of Japan.

*Correspondence to: Masafumi Taniwaki MD, PhD, Department of Molecular Hematology and Oncology, Kyoto Prefectural University of Medicine Graduate School of Medical Science, 465 Kajii-cho, Kawaramachi-hirokoji, Kamigyo-ku, Kyoto 602-8566, Japan. E-mail: taniwaki@koto.kpu-m.ac.jp

Received 13 August 2013; Accepted 5 December 2013
DOI 10.1002/gcc.22140
Published online 21 January 2014 in Wiley Online Library (wileyonlinelibrary.com).

KAT6A-EP300 (adenoviral EIA-associated protein *p300*) in t(8;22)(p11;q13) (Chaffanet et al., 2000), and *KAT6A-NCOA3* (nuclear receptor coactivator 3, also known as *TRAM-1*, *RAC3*, *pCIP*, or *AIB-1*) in t(8;20)(p11;q13) (Esteyries et al., 2008). These fusion genes produce the same disease pattern with blast cells of a monocytoid phenotype. Previous studies have revealed that *KAT6A* is essential for the self-renewal of hematopoietic stem cells (Katsumoto et al., 2006; Thomas et al., 2006), and KAT6A fusion proteins enable the transformation of non-self-renewing myeloid progenitors into leukemia stem cells (Huntly et al., 2004). Other data have shown that *KAT6A* cooperates with *MLL* to regulate *HOX* gene expression in human cord blood CD34+ cells (Paggetti et al., 2010). In the present study, a case of therapy-related AML with t(8;19)(p11;q13) was analyzed and a novel *KAT6A* fusion partner was identified using the cDNA bubble PCR method.

MATERIALS AND METHODS

Patient

A 71-year-old male was initially diagnosed as having non-Hodgkin's lymphoma (diffuse large B-cell lymphoma, DLBCL, stage IIIA, IPI: high-intermediate). He was treated with six cycles of chemotherapy consisting of R-THP-COP (rituximab, pirarubicin, cyclophosphamide, vincristine, and prednisolone), after which partial remission was obtained. Six months after treatment initiation, he presented to the hospital complaining of general malaise and dyspnea. Complete blood cell count on admission demonstrated elevated white blood cell count (6.62×10^9/l, 44% blast) and thrombocytopenia (46×10^9/l). Bone marrow aspirate showed 78.4% blast cells, and cytochemical studies revealed that the blast cells were positive for myeloperoxidase, non-specific esterase (butyrate esterase), and specific esterase (chloroacetate esterase). He was diagnosed as having AML (FAB M4). Flow cytometric study also revealed that the vast majority of leukemic cells were positive for CD4, CD13, CD33, CD56, and HLA-DR, and high serum and urine lysozyme levels were observed (28.9 mg/l and 0.4 mg/l, respectively). These findings were also consistent with AML (FAB M4). Erythrophagocytosis was observed in bone marrow smears; however, extramedullary involvement was not observed. Other significant laboratory data included elevated lactate dehydrogenase (LDH) of 2,093 IU/l, fibrin degradation product (FDP) of 21.6 μg/ml, and D-dimer of 16.9 ng/ml, which suggested disseminated intravascular coagulation (DIC). The patient did not respond to induction chemotherapy with idarubicin and cytarabine, but responded partially to second line therapy with gemtuzumab ozogamicin. However, he died four months after the diagnosis of AML because of leukemia progression. After informed consent was obtained from the patient, the leukemic cells at diagnosis were analyzed. The Institutional Review Board of Kyoto Prefectural University of Medicine approved this study.

Spectral Karyotyping Analysis

Spectral karyotyping (SKY) analysis was performed with a Sky Painting kit (Applied Spectral Imaging, MigdalHa'Emek, Israel). Signal detection was performed according to the manufacturer's instructions.

Fluorescence In Situ Hybridization Analysis

Fluorescence in situ hybridization (FISH) analysis using *KAT6A*-specific BAC clones (RP11–45I11, 3′ of *KAT6A* and RP11–589C21, 5′ of *KAT6A*) was carried out as previously described (Taniwaki et al., 1994).

cDNA Bubble PCR

cDNA bubble PCR was conducted as previously described (Chinen et al., 2008), and its outline is shown in Figure 1. The sequences of all primers used in this study are listed in Table 1. Nested PCR was performed using the primers NVAMP-1 (bubble oligo) and MOZ-E16-1S for first-round PCR, and NVAMP-2 (bubble oligo) and MOZ-E16-2S for nested PCR. Poly(A)+ RNA was extracted from the patient's leukemic cells using the QuickPrep Micro mRNA Purification Kit (GE Healthcare, Waukesha, WI).

Bubble PCR of Genomic DNA

Bubble PCR of genomic DNA was performed as previously described (Smith, 1992; Zhang et al., 1995). Primers used were as follows: NVAMP-1 and MOZ-GNM2S1 for first-round PCR, and NVAMP-2 and MOZ-GNM2S2 for second-round PCR (Table 1).

RT-PCR and Genomic PCR Analyses

RT-PCR and genomic PCR analyses were performed as previously described (Chinen et al.,

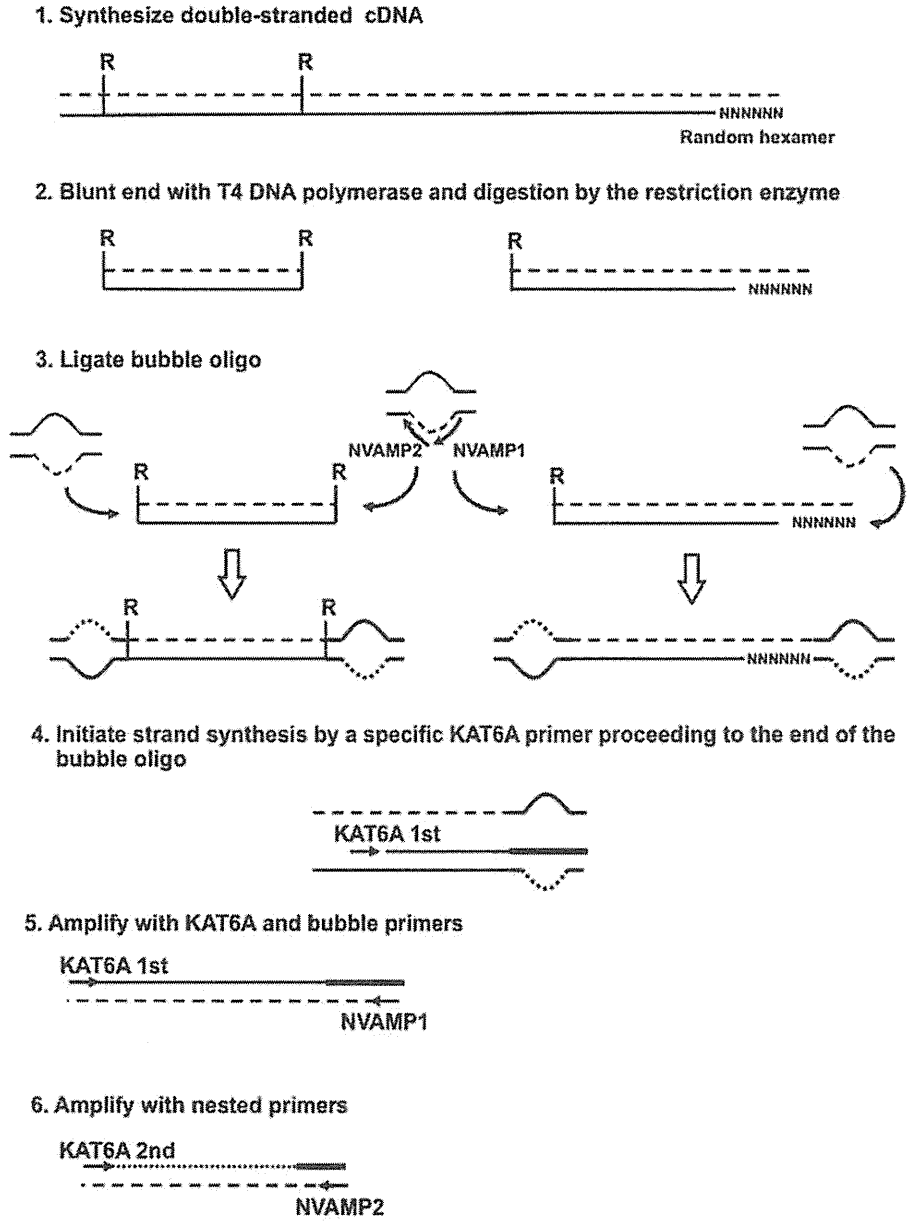

Figure 1. Outline of cDNA bubble PCR. Bubble PCR primers (NVAMP-1 and NVAMP-2) can only anneal with one complementary sequence for bubble oligo synthesized with *KAT6A* primer but not bubble oligo itself; therefore, this single-stranded bubble provides the specificity of the reaction. The sequences of primers used are listed in Table 1. Nested PCR was performed using primers NVAMP-1 (bubble oligo) and MOZ-E16-1S for 1st round PCR, and NVAMP-2 (bubble oligo) and MOZ-E16-2S for nested PCR for the detection of *KAT6A-LEUTX* fusion transcripts, and primers NVAMP-1 and MOZ-GNM2S1 for 1st round PCR, and NVAMP-2 and MOZ-GNM2S2 for nested PCR for the detection of *KAT6A-LEUTX* genomic fusion point. NVAMP1 and NVAMP2 can only anneal to the newly synthesized unique sequence of the bubble oligo by MOZ-E16-1S.

2008). After 35 rounds of PCR (30 s at 94°C, 30 s at 55°C, and 1 min at 72°C), 5 μl of PCR product was electrophoresed in a 3% agarose gel. Primer pairs were as follows: MOZ-E16-1S/MF19-1AS and MOZ-3A/MF19-1S for RT-PCR; MOZ-GNM2S2/MF19-GNM2A and MF19-GNM2S/MOZ-GNM2A for genomic PCR; MOZ-E16-1S/LEUTX-5A for RT-PCR to detect whole sequence of *LEUTX* in the chimeric transcript (Table 1).

Nucleotide Sequencing

Nucleotide sequences of PCR products and, if necessary, subcloned PCR products were analyzed as previously described (Chinen et al., 2008).

Expression Analysis of LEUTX *in Normal Tissues*

Pre-made Northern blots (human 12 lane MTN blot, Clontech, Palo Alto, CA) were hybridized to probes labeled using the Dig-labeled PCR method according to the manufacturer's instructions (Roche Applied Science, Gilroy, CA). Probes were 112 bp *LEUTX* cDNA fragments (nucleotides 166–667; GenBank accession no. NM_001143832). Human 1st strand cDNA Mix was used for RT-PCR (Genostaff, Tokyo, Japan).

TABLE I. Primers Used in This Study

Forward primers	
MOZ-E16-1S	GGTGTCAGTCCTCTTCTAAG
MOZ-E16-2S	GATGAAGAGTCAGATGATGCTG
MOZ-GNM2S1	CCCTGATTAAGTTCCCATGG
MOZ-GNM2S2	TTGCTGATGCAGCCATTTCC
MF19-1S	CACACGGTTTTCAGCCTCAT
MF19-GNM2S	TCCCTTCAGTCTCTCACCCA
Reverse primers	
MF19-1AS	AGTCTCCTCCTTCTTCACTG
MOZ-3A	GCGTCATTGAGCCCATCGTTTCCA
MF19-GNM2A	CCAGTGGCAGAACAGTGAAT
MOZ-GNM2A	TACTCTAGGCCATGACTGAG
LEUTX-5A	TTACACTGAAGATTGGAGCTGG
Bubble PCR primers	
NVAMP1	TGCTCGTAGTAATCGTTCGCAC
NVAMP2	GTTCGCACGAGAATCGCAAGAT

RESULTS

Identification of the KAT6A-LEUTX *Fusion Transcript*

G-banding of the leukemic cells of the patient revealed 46,XY,t(8;19)(p11;q13) in all 20 cells analyzed, and it was confirmed by SKY (Fig. 2A). Because the patient was diagnosed as having AML-M4 with hemophagocytosis, and not a myeloproliferative neoplasm, a *KAT6A* rearrangement was thought more likely than an *FGFR1* rearrangement. FISH analysis using *KAT6A*-specific BAC clones

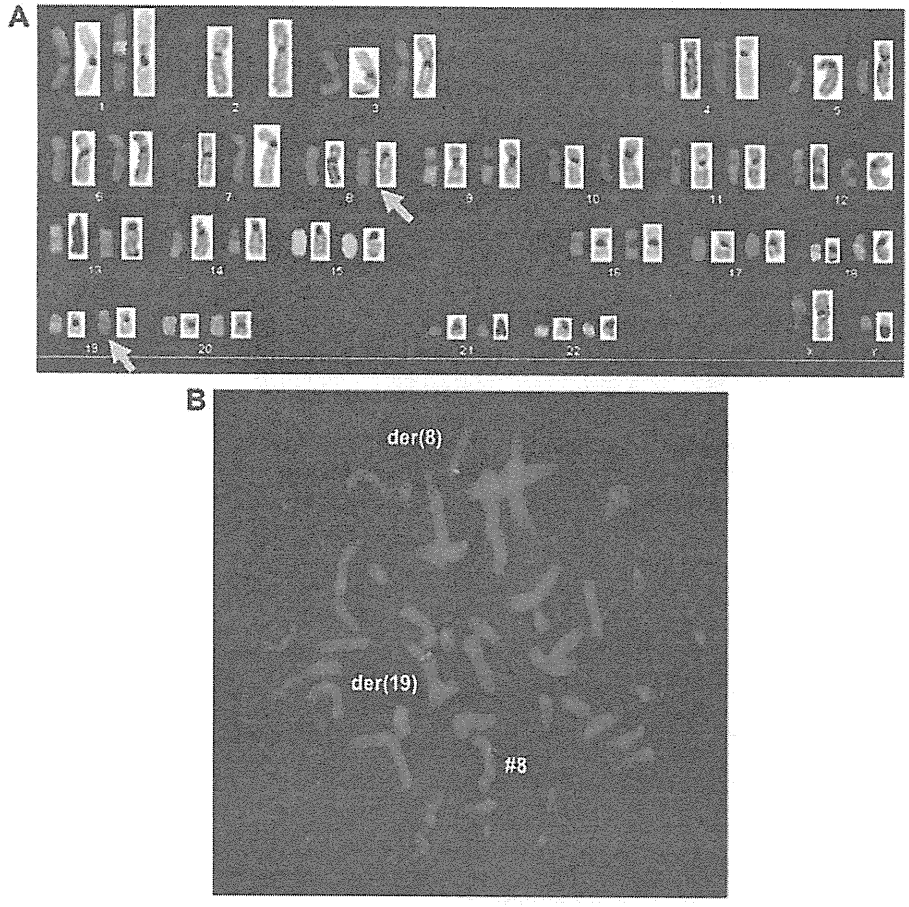

Figure 2. A: SKY analysis. Arrows indicate rearranged chromosomes. B: FISH analysis. RP11–5B9C11 (green, 3′ side of *KAT6A*) and RP11–451I1 (red, 5′ side of *KAT6A*). One fusion signal was detected on chromosome 8.

showed *KAT6A* split signals on der(8) and der(19) (Fig. 2B). The cDNA bubble PCR method was performed to identify the *KAT6A* fusion partner. Products of various sizes were obtained (Fig. 3A), and one product contained a 25 bp *KAT6A* sequence fused to an 84 bp unknown sequence (Fig. 3B). Initially, a BLAST search revealed that the unknown sequence was identical to that of a gene encoding a hypothetical protein identified from a human placenta cDNA library (GenBank accession no. CR746510); later, that sequence was shown to be part of the *LEUTX* (leucine twenty homeobox) gene (GenBank accession no. NR_003931). RT-PCR confirmed the in-frame fusion transcript of the exon 16 of *KAT6A* and exon 2 of *LEUTX* (Fig. 3C). The NCBI database showed that the *LEUTX* gene consists of three exons; however, the predicted amino acid sequence of *LEUTX* exon 1 continues in frame into exon 2 (Fig. 4). Although we attempted to find upstream *LEUTX* sequences, no upstream exon could be identified by bubble PCR. Another RT-PCR to detect the fusion transcripts contained whole sequence from exon 2 and to the stop codon of exon 3 were amplified (Fig. 3D).

Detection of KAT6A-LEUTX Genomic Junctions

To isolate the fusion point of chromosomes 8 and 19, bubble PCR was performed on genomic DNA previously digested with *Hae*III, and nested PCR products were detected using the primers MOZ-GNM2S2 and NVAMP2 (Fig. 5A). Sequence analysis of the subcloned PCR product revealed the genomic junction of 5′-*KAT6A-LEUTX*−3′, and the result was confirmed by PCR analysis using the primers MOZ-GNM2S2 and MF19-GNM2A (Fig. 5B). Bubble PCR on genomic DNA revealed that the genomic breakpoints were within intron 16 of *KAT6A* and 4,314 bp upstream of the known first exon of *LEUTX* (Fig. 5C). The fusion products of exon 1 of *LEUTX* and exon 16 of *KAT6A* were not detected by RT-PCR.

Expression of the LEUTX Gene

To examine the expression of the *LEUTX* gene at the RNA level, Northern blot analysis was performed using the *LEUTX* cDNA probe spanning exons 2–3. *LEUTX* RNA could not be detected in 12 various human tissues (including brain, heart, skeletal muscle, colon, thymus, spleen, kidney,

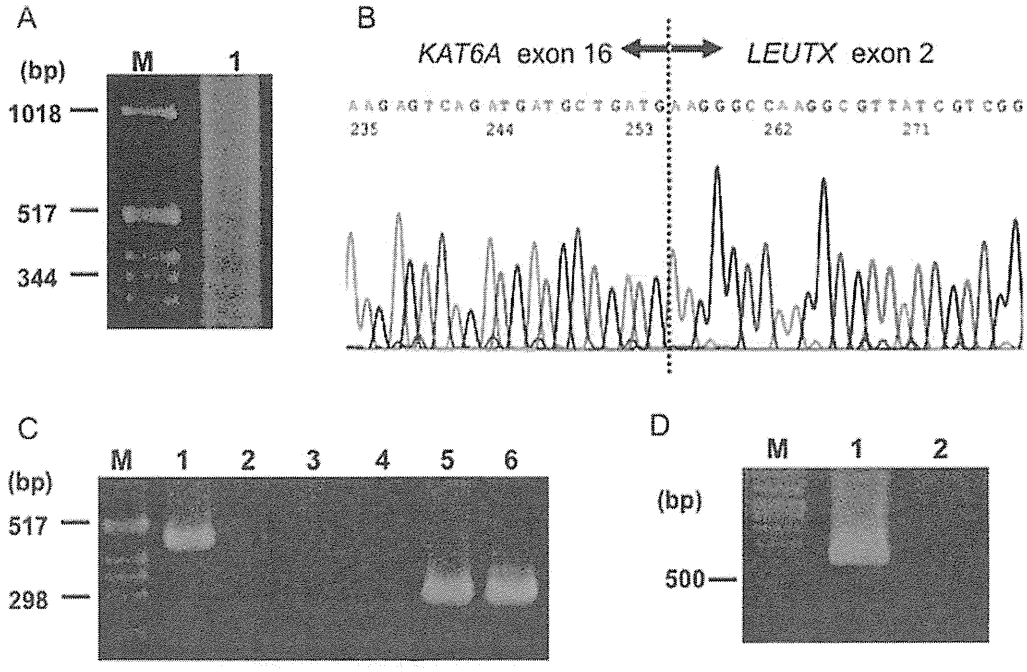

Figure 3. Identification of *KAT6A-LEUTX* fusion transcript. A: Bubble PCR products by nested PCR using MOZ-E16-1S and NVAMP1 for the 1st PCR, and MOZ-E16-2S and NVAMP2 for the 2nd PCR (lane 1). M, size marker. B: Sequence analysis of *KAT6A-LEUTX* fusion transcript. C: Detection of *KAT6A-LEUTX* fusion transcripts by RT-PCR. Primers used are: MOZ-E16-1S and MF19-1AS for 5′-*KAT6A-LEUTX*−3′ (lanes 1 and 2); MF19-1S and MOZ-3A for reciprocal fusion transcripts (lanes 3 and 4), and primers for β-actin (lanes 5 and 6). Lanes 1, 3, and 5, patient's leukemic cells; lanes 2, 4, and 6, normal peripheral lymphocytes. D: Detection of *KAT6A-LEUTX* fusion transcripts with a primer containing the stop codon of *LEUTX* by RT-PCR. Primers used are: MOZ-E16-1S and LEUTX-5A. Lane 1, patient's leukemic cells; lane 2, water; M, size marker.

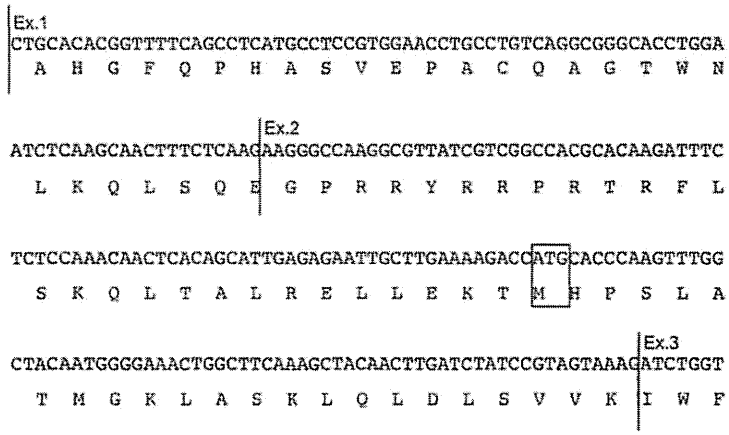

Figure 4. Partial sequencing of *LEUTX* cDNA. The NCBI database (GenBank accession no. NR_003931) shows that the *LEUTX* gene consists of three exons, and that the boxed ATG in exon 2 is the translation initiation codon of *LEUTX*; however, the frame is open all of the way to 5′ end of exon 1. Although we attempted to find upstream *LEUTX* sequences, no sequences could be identified by bubble PCR.

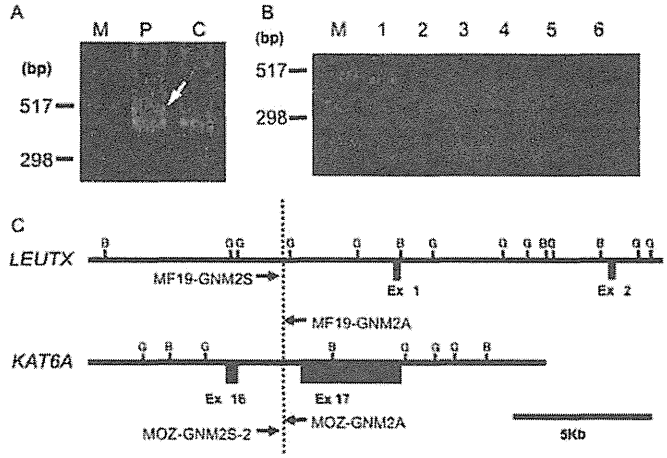

Figure 5. Cloning of the genomic junction of *KAT6A* and *LEUTX*. A: Bubble PCR for genomic DNA. P, patient's leukemic cells; N, normal peripheral lymphocytes. B: Detection of the genomic fusion point of *KAT6A-LEUTX* by PCR. Primers used are MOZ-GNM2S-2 and MF19-GNM2A (lanes 1–3), and MF19-GNM2S and MOZ-GNM2A (lanes 4–6). Lanes 1 and 4, patient's leukemic cells; lanes 2 and 5, leukemic cell line PEER; lanes 3 and 6, water. M, size marker. C: Physical map of the breakpoint regions. Black boxes represent defined exons in each gene. Horizontal arrows show the primers used. Restriction sites are indicated by capital letters: G, *Bgl*II; B, *Bam*HI.

liver, small intestine, placenta, lung, and peripheral blood leukocytes). RT-PCR with the human cDNA mix with 12 tissues (including brain, heart, liver, lung, kidney, stomach, small intestine, large intestine, muscle, spleen, placenta, and testis) also could not detect any *LEUTX* gene transcript. Since the NCBI expressed sequence tag (EST) database showed that *LEUTX* was expressed only in placenta, RT-PCR was performed using human placental total RNA (Clontech, Palo Alto, CA) as template, which finally revealed the normal *LEUTX* transcript. No expression of the *LEUTX* transcript was found in any leukemic cell line, such as Kasumi-3, ML-1, LAZ-22, TS 9;22, or THP-6 (data not shown).

DISCUSSION

This study identified a novel *KAT6A-LEUTX* fusion gene in a patient with therapy-related AML (FAB-M4) with t(8;19)(p11;q13). This is the sixth, but unique, *KAT6A* fusion partner which does not have a HAT domain (Fig. 5). Several previous studies have reported AML-M4 or M5 cases with t(8;19)(p11;q13) (Brizard et al., 1988; Stark et al., 1995), and a *KAT6A* rearrangement was detected

in an AML-M5 with t(8;19)(p11;q13) (Gervais et al., 2008), suggesting that this fusion is recurrent. To date, five genes have been identified as *KAT6A* fusion partners in translocations including *CREBBP*, *EP300*, *NCOA2*, *NCOA3*, and *ASXL2* in leukemia (GenBank accession no. AB084281) (Imamura et al., 2003) (Fig. 6). *LEUTX* and *ASXL2* differ from the other fusion partner genes, in terms of molecular characteristics. The remaining four have a histone acetyltransferase (HAT) domain, whereas *LEUTX* and *ASXL2* do not (Katoh and Katoh, 2004). *ASXL2* may theoretically interact with histone-modifying enzymes because its homolog is *ASXL1*, modulates the activity of *LSD1*, a histone demethylase of H3K4 and H3K9, by cooperation with heterochromatin protein-1 (*HP1*) (Wang et al., 2009; Lee et al., 2010). The sequence of the *LEUTX* gene contained in the *KAT6A-LEUTX* chimeric transcript is shorter than that of the other partner genes involved in *KAT6A* translocations, suggesting a different mechanism of leukemogenesis.

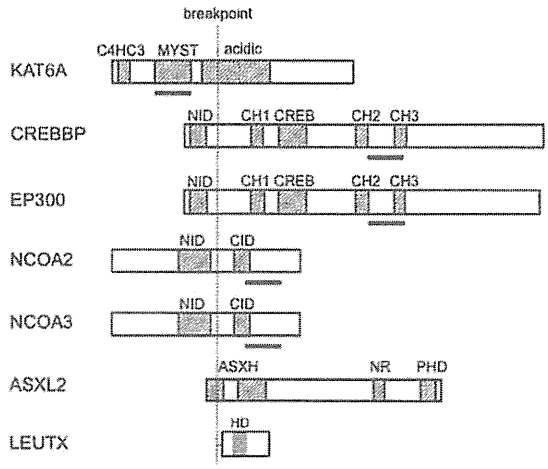

Figure 6. Schematic representation of putative KAT6A, LEUTX, and other KAT6A fusion proteins. C4HC3, zinc finger domain associated with chromatin binding; MYST, MYST domain; Acidic, Acidic domain; NID, nuclear hormone receptor interaction domain; CH 1–3, cysteine/histidine-rich domains 1–3; CREB, cyclic-AMP response element binding protein domain; CID, CBP-interacting domains; ASXH, ASX homology domain; NR, nuclear receptor box; PHD, plant homeodomain; HD, homeodomain; Horizontal bars, Regions of HAT domain.

LEUTX is characterized by the presence of a leucine residue at the otherwise highly conserved homeodomain position 20 (Holland et al., 2007). Although *LEUTX* is one of the homeobox genes, the translated protein has never been recorded in the NCBI database. However, *LEUTX* is potentially a protein-coding gene, based on previously reported findings. Firstly, *LEUTX* is highly conserved and necessary for placental mammals except rodents (Zhong and Holland, 2011). Secondly, the NCBI database now shows that *LEUTX* is expressed only in placental tissue. Our data by Northern blotting and RT-PCR also confirmed this. A previous report showed that thousands of genes are transcribed at a rate of only one copy per cell, yet do perform functions (Kuznetsov et al., 2002). These data strongly suggest that *LEUTX* is associated with the formation of the placenta. Thirdly, *LEUTX* is considered to arise by tandem duplication and extreme divergence from *CRX* (Zhong and Holland, 2011), which is a member of the *Otx* gene family interacting with *CREBBP*, *EP300*, and *NCOA2* (Yanagi et al., 2000), based on its localization close to the PRD-class genes *TPRX1*, *CRX*, *DPRX*, and *DUXA* on the distal end of the long arm of chromosome 19. These data suggest that *LEUTX* may function as a homeobox gene. Fourthly, a previous study of *NKX2.6* gene confirmed that the missense mutation of F151L at position 20 in the homeodomain reduced its transcriptional activation (Heathcote et al., 2005). This data suggests that leucine, but not phenylalanine, in LEUTX alters and reserves the transcriptional activity of the homeodomain protein. Finally, a KAT6A fusion partner *per se* may play a role in leukemogenesis, because a mutant KAT6A protein, transcribed from the truncated N-terminal part of KAT6A sequence within KAT6A-NCOA2, did not bind CREBBP in contrast to the full length KAT6A or KAT6A-NCOA2 protein in vitro (Collins et al., 2006).

```
                                    RNYNNCNNGYNGKTNYNY
                                    ******* ****** **
KAT6A          AAAATTTTAAGTTTTATGTTACGTATAGTTTACCATAGTTTTTTTAAAAATG
               ||||||||||||||||||||||||||||
KAT6A-LEUTX    AAAATTTTAAGTTTTATGTTACGTAAAAGTCACTCATGCTAAATGCCACATT
                                           ||||||||||||||||||||||||||||
LEUTX          CCAACGGACCAGACCAAACCAAAATAAAGTCACTCATGCTAAATGCCACATT
```

Figure 7. DNA sequences across the junction points of *KAT6A* and *LEUTX*. Topoisomerase II recognition site-like sequences (5′-RNYNNCNNGYNGKTNYNY-3′) near the junction points are aligned. R, purine; Y, pyrimidine; N, any base; K, G or T; and *, homology.